Kinetics of iron electrochemical reduction into liquid metal at 1823 K in a molten oxide electrolyte

Jan Wiencke, Hervé Lavelaine, Gavin John Kane, Pierre-Jean Panteix, Carine Petitjean, Christophe Rapin

Kinetics of iron electrochemical reduction into liquid metal at 1823 K in a molten oxide electrolyte

Jan Wiencke*[1,3], Hervé Lavelaine[1], Gavin John Kane[2] Pierre-Jean Panteix[3], Carine Petitjean [3], Christophe Rapin[3]

** Corresponding author, Email-address: Jan.wiencke@arcelormittal.com*

[1] Ironmaking, Maizières Process, Global Research and Development ArcelorMittal, Voie Romaine, B.P. 30320, 57283 Maizières-lès-Metz, Cedex, France

[2] I2AR, University of Applied Science Emden Leer, 276724 Emden, Germany

[3] IJL-UMR 7198, Université de Lorraine Département CP2S, Equipe 206 (Surface et Interface: Réactivité Chimique des Matériaux), B.P. 70239-F-54506 Vandoeuvre les Nancy Cedex, France

Abstract

The kinetic parameters of the electrochemical reduction of iron oxide into liquid iron metal in a molten oxide electrolyte were measured at 1823 K. A large surface anode was used to circumvent the need of a reference electrode and a stepped linear scan voltammetry was applied to an iron-bearing silicate electrolyte over a cell-voltage range of 0.8 V to 1.9 V.

The cathode half-reaction identified by this method is the reduction of ferrous iron into its metal state. In order to extract the kinetic parameters the current response is treated concerning the electronic charge transfer and the ohmic drop due to the electrolyte in the electrochemical cell. Derived parameters imply that electrode kinetics follow Tafel behavior. An order of reaction close to unity with transfer coefficients between 0.54 and 0.66 is identified.

Keywords: molten oxides, kinetics of liquid iron production, large surface electrode, silicates

1. Introduction

Molten oxide electrolysis (MOE) is one of the possible routes for direct extraction of metals from their ores [1] [2]. Its main advantage relies in the production of oxygen gas as the sole byproduct as opposed to carbon dioxide in the case of conventional metal production routes. Metal extraction from natural resources is accomplished in MOE by the electrochemical separation of metal oxides into the reference phases of its elements:

$$MO_{(l)} \rightarrow M_{(s,l)} + \tfrac{1}{2}\, O_{2(g)} \qquad (1)$$

Although the first investigated use of this method was the production of oxygen on the moon [3], this technique has shown high potential for the industrial production of iron metal without the negative side effect of the production of greenhouse gases such as CO_2 [1] [4]. During the last decade effort was mainly focused on the identification of a suitable anode material, withstanding temperatures above 1823 K and oxidizing conditions with $P(O_2)$ close to unity [4] [5] [6] [7] [8]. As main focus in these studies was the anode half-cell reaction, the cathode reaction, which produced an iron-molybdenum alloy, was not further specified. The cathode half-reaction yielding metal production can thus either be the reduction of ferrous iron following

$$Fe(II) + 2e^- \rightarrow Fe^0 \qquad (2)$$

or the reduction of ferric iron by

$$Fe(III) + 2e^- \rightarrow Fe^0 \qquad (3)$$

The purity of the electrochemical nature of the reduction process at the cathode, when using a molybdenum electrode, has however to be strongly questioned. The metal is chemically oxidized by the melt and the cathode half-cell reaction thus compromised [9]. Up to this point the description of the process of cathodic reduction of Fe(II) to liquid

metallic iron is uncharacterized despite being one of the most important industrial redox reactions in terms of yearly mass and energy involvement worldwide. Providing the kinetic parameters of the reaction is paramount to further engineering development of this processing route [10]. The relation between production rate and electric tension is necessary to design an energy balanced process and to choose the conditions for maximum selectivity of the reaction. In order to answer to this essential requirement, this study is aimed at defining the cathode half- cell reaction and to obtain information about the corresponding mechanism (diffusion, charge transfer) and kinetics (resistance to interfacial charge transfer) of the process.

Usually the different kinetic parameters are measured separately with a 3-electrodes set-up using a reference electrode. However at operating temperatures of MOE a reference electrode is not defined to this point. Although Molybdenum has been used as a reference electrode for MOE in literature, e.g. in references [7] and [8], it is deemed unsuitable due to the before mentioned chemical reaction of the metal with the molten oxide. The corresponding equilibrium of Molybdenum and the melt would suffer an evolution with time and thus an identification of the kinetic parameters of the cathode half-cell reaction would be compromised.

In this work the cathode half-reaction is studied by the means of a stepped linear scan voltammetry. A corresponding typical “I vs. E”-plot, which can be obtained in a silica-slag, is shown in Figure 1 (a). In the case of Figure 1 (a), the anode and the cathode have similar dimensions. When imposing a potential between the two electrodes $\Delta E = | E_C - E_A |$, the resulting anodic and cathodic current must be equal: $i_A = | i_C |$. In this case, the decomposition of the imposed potential in the cell depends on both, the anode- and the cathode-side.

The use of a Large Surface Anode (LSA) can be useful in order to get access to cathodic process parameters. Here the anode surface is much greater than the cathode surface. The anodic current (product of current density and electrode surface) will then be independent of the potential, as can be seen in Figure 1 (b). Consequently, when the potential imposed between anode and cathode increases from $\Delta E_1 = | E_{C1} - E_{A1} |$ to $\Delta E_2 = | E_{C2} - E_{A2} |$, the evolution of the potential will mainly depend on the cathodic part E_C as anodic parts, E_{A1} and $E_{A2,}$ will have very close values. The shift of E_A in this configuration is thus negligible in comparison to the shift of $E_{C.}$ Hence the use of a large surface anode is a way to control the cathodic potential in a two electrodes device.

In the work proposed here, silica based slags with various iron contents are characterized by means of a large surface anode and stepped linear scan voltammetry in order to describe to the rate limiting steps of iron reduction.

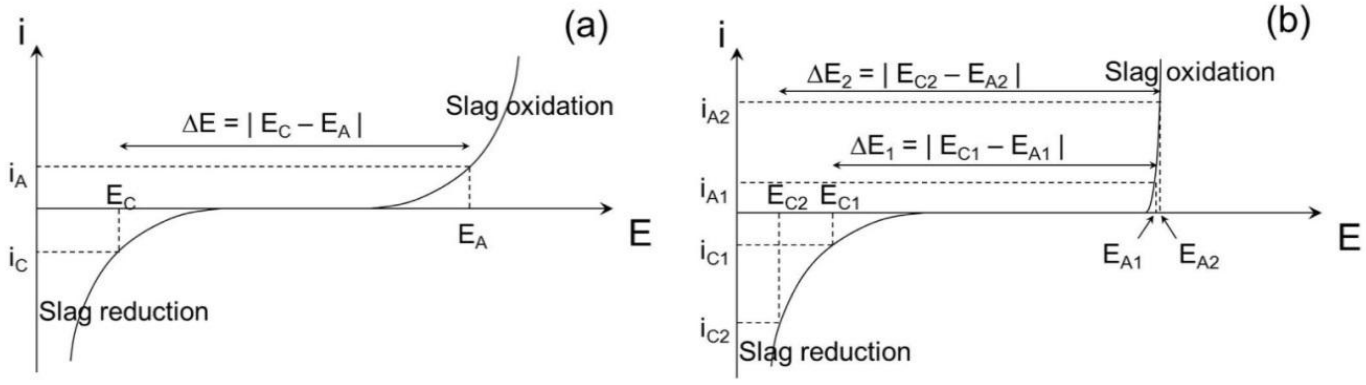

Figure 1: Typical current vs. potential plot of a silica based slag.
Measurements performed with anode and cathode with similar dimensions (a), and with large surface anode (b).

2. Experimental setup

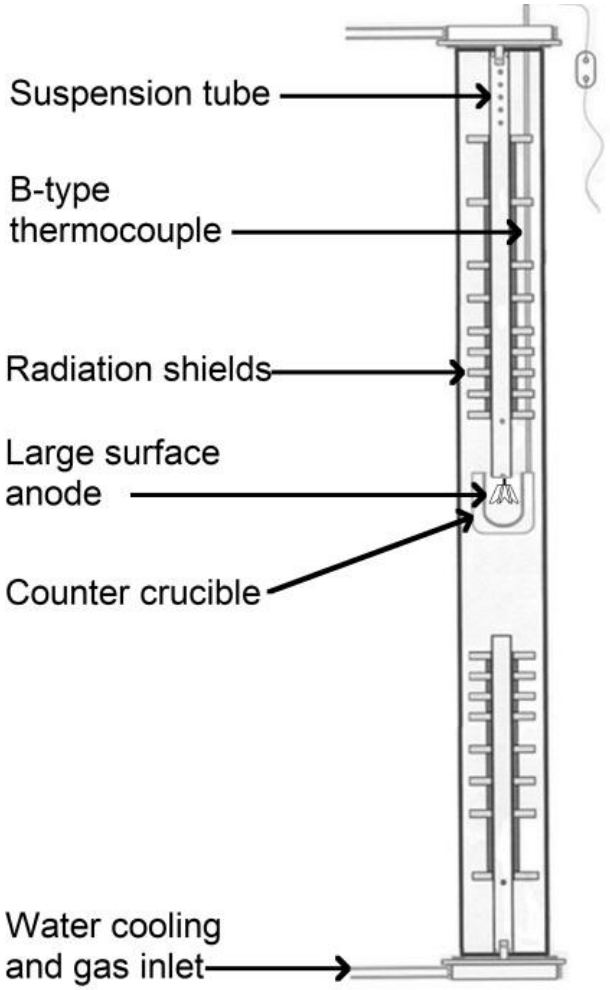

Figure 2: *Schematic drawing of experimental setup*
Assemblage in tube furnace (not to scale);Tube-Height: 150 cm; outer Tube-diameter: 8.6 cm

Experiments were conducted in a vertical tube furnace, which was flushed with an Argon gas flow (Figure 2). The electrochemical cell was placed therein and the electrochemical measurements were performed in the isothermal region of the tube furnace. Alumina is chosen as a refractory material for the crucible. Acquisition of the temperature was performed *via* a B-type thermocouple, positioned directly next to the cell. Electrolytes for the experiments were prepared from oxide powders and mixed manually. The resistance

of the wiring in the cell and the furnace was measured in a reference trial at same temperature as the electrochemical experiments. Electrodes were short-circuited and the resistance then determined as 0.8 Ohm.

Concerning the anode, its large surface must have a stable geometry throughout the experimental duration of several hours. Necessity for this exists due to the requirement of a constant cell factor for the derivation of the cell resistance. Use of conventional electrode geometries, such as that of a disk or a plate, are accordingly avoided, as their rim would likely creep with time under their own weight. The chosen device, made from a Pt-10%Rh alloy, is shown in Figure 3. Besides the geometrical stability it also offers an easy evacuation of gas bubbles generated during the electrochemical experiments. The fins of the LSA are designed in a manner that they form a hemisphere concentric with the cathode, so that the ohmic resistance is low and the current distribution between the electrodes is kept as homogeneous as possible on both electrodes. The surface of the anode immerged in the molten oxide is 3350 mm^2. The cathode, which is a Pt-30%Rh wire, protrudes the crucible and extends into the molten oxide with a surface of 6 mm^2. Distance between the electrodes is 15 mm. The geometry of the experimental cell is modeled using “Computer-Aided-Design” software (Creo Elements by PTC) to obtain its geometric factor K by means of the Laplace equation with constant potential on electrodes, a net-flux equal to zero on insulating surfaces and assuming uniform electrical conductivity,

$$\Delta\varphi = 0 \qquad (4)$$

where Δ is the Laplacian operator and φ the electrical potential in the electrolyte. Data analysis was performed by Mathworks® and the included “Partial Differential Equation”-toolbox. The value hereby obtained is K = 0.46 cm^{-1}. The equipotential surfaces in the cell are displayed in Figure 4 to illustrate the distribution of the ohmic drop in the cell. It shows from this illustration that most of the potential drop in the cell is located close to the cathode. This verifies the approach of using the large surface anode to describe the cathodic resistance, as the current densities obtained at the anode, and thus its respective electrochemical kinetic resistance, are negligible in comparison.

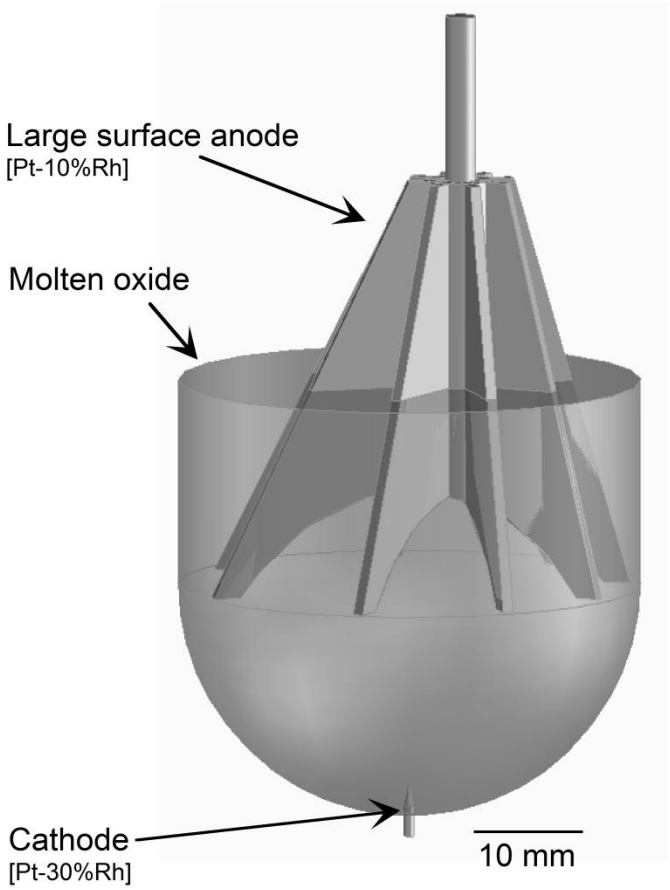

Figure 3: 3D illustration of the electrochemical setup including the Large Surface Anode

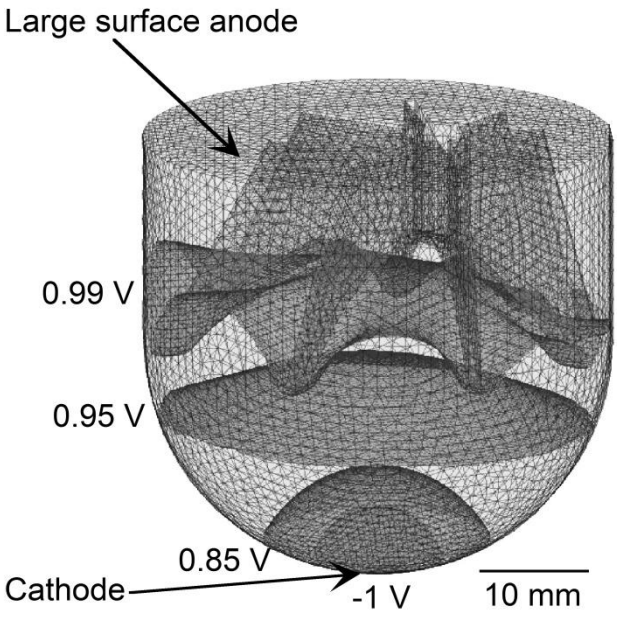

Figure 4: Illustration of the equi-potential lines in the electrolyte

The electrolyte investigated in this study is based on a mixture of silica (66 wt%), alumina (20 wt%) and magnesia (14 wt%) to which iron oxide is added in different quantities as magnetite. Reasoning for the choice of this base composition is the inherent low quantity of ferric iron due to the high silica content [9] [11] [12] [13] as well as the low liquidus temperature of 1350°C [14]. In comparisons, molten oxides with a high optical basicity, such as CaO-based slags, stabilize the highest oxidation degrees [9]. The choice of such a composition would lead to a high proportion of ferric iron in the melt and is thus avoided. Quantity of ferric iron in the slag is calculated with the thermochemical software CEQCSI [14]. The ratio between the molar fraction of Fe(III) and the total Fe molar quantity in the melt defines the ferric ratio

$$\#Fe(III) = \frac{Fe(III)}{Fe(total)} \qquad (5)$$

In the molten oxides used in this study #Fe(III) ranges from 0.001 to 0.0016. Table 1 summarizes the compositions and properties of the electrolytes investigated in this work.

Table 1: Composition, ferric ratio, liquidus temperature and density of the electrolytes analyzed in this study

	SiO_2 [wt%]	Al_2O_3 [wt%]	MgO [wt%]	FeO_x [wt%]	#Fe(III)[1)]	Liquidus Temperature[2)] [K]	Density[3)] [kg m^{-3}]
Fe#5	62.7	19.0	13.3	5.0	0.0010	1570	2622
Fe#7.5	61.0	18.5	13.0	7.5	0.0012	1543	2660
Fe#10	59.4	18.0	12.6	10.0	0.0013	1534	2698
Fe#15	56.1	17.0	11.9	15.0	0.0016	1540	2777

[1)] Calculated by CEQCSI [14]; Conditions: 1823 K in equilibrium with iron metal
[2)] Calculated by CEQCSI [14] for equilibrium with iron metal
[3)] Calculated following [15]

To describe the kinetics of the cathode half-reaction a stepped linear scan voltammetry is conducted. Choice of the cell voltage interval is based on the intention to address the reduction of iron species at the cathode. Hence, the lower limit of this interval has to be chosen slightly below the reduction potential of iron oxide and the upper limit is just below the reduction potential of silica. As the magnitude of current is unknown before the actual trial the corresponding ohmic drop in the cell has to be estimated. This affects the upper limit of the cell voltage range to the extent that it can be defined at higher values. Accordingly, the voltage range selected is 0.8 to 1.9V. A step-duration is fixed at 10 min, which allows an *in-situ* quantification of the anodic oxygen-evolution-reaction. The total duration of the linear scan is 560 min.

Once the furnace had cooled down naturally, the experimental cells were recovered and the cathode wires and metal deposits extracted. The deposits were embedded in resin, polished (finishing grade: 1µm with diamond solution) and subsequently analyzed via scanning electron microscopy using a field emission JEOL JSM 7800F. The device is equipped with a field emission gun (FEG) using a Schottky-emitter. Qualitative analysis was done with an energy-dispersive spectrometer (EDS) installed on the electron microscope.

3. Experimental plan

3.1. The electrochemical decomposition of the cell voltage in two-electrodes cells

During stepped linear scan voltammetry performed with a two-electrodes setup a cell voltage is applied onto the electrolyte. The applied cell voltage ΔV includes different contributions according to the following relation:

$$\Delta V = \Delta E_F + R_T i + R_{MO} i + \eta_A + \eta_C \quad (6)$$

where ΔE_F is the thermodynamic potential of the redox-reaction [V], i the current passed through the cell [A], R_T the terminal resistance of the installation imposed by wires connecting the cell to the electrical source [Ω], R_{MO} the ohmic resistance of the electrolyte in the volume of electrolyte connecting the electrodes [Ω], η_A the overpotential of the anodic half-reaction [V] and η_C the overpotential of the cathodic half-reaction [V] [16]. This equation allows the determination of the cathode overpotential by determining the remaining terms on the right hand side. These can be identified independently from each other.

For faradaic charge transfer to take place in the cell, the cell voltage must surpass a thermodynamic threshold [16]. This threshold is defined by the electrochemical reactions occurring at the interface of the electrodes and the electrolyte. It is deduced from the Gibbs free energy of the redox-reaction taking place at constant temperature and pressure:

$$\Delta E_F = \frac{\Delta G^0}{nF} + \frac{RT}{nF} ln\left[\Pi_i a_i^{\nu i}\right] \quad (7)$$

where ΔG^0 is the standard Gibbs free energy of the considered reaction in pure component state [J mol^{-1}], F Faraday's constant [C mol^{-1}], $\Pi_i a_i^{vi}$ is the activity product with v_i the stoichiometric coefficient of compound "i", n the number of electrons involved in the reaction, T the temperature [K] and R the universal gas constant [J mol^{-1} K^{-1}].

The overpotentials at the electrodes can be understood as a contact resistance between the electrode and the electrolyte caused by the polarization of both due to the application of a cell voltage

3.2. Treatment of the acquired current response during the electrochemical analysis

The aim of this paragraph is the presentation of the methodology used in this study to correct cell voltage from the independent contributions of i) the terminal resistance R_T of the wiring and ii) the overall ohmic drop $R_{MO}i$ in the electrolyte.

As a first step, i), the effect on the cell voltage (ΔV) due to the terminal resistance of the complete installation, R_T = 0.8 Ω, is taken into account to obtain the voltage drop that occurs in the electrolyte (ΔV_E). This is performed *via*

$$\Delta V_E = \Delta V - (iR_T) \quad . \qquad (8)$$

In the second step, ii-1) the total current i is corrected of the electronic contribution i_E. This charge transfer, i_E, corresponds to the electronic conduction in the electrolyte as well as the electron transfer due to a possible ferrous-ferric loop between the electrodes. The latter defines the oxidation of ferrous iron at the anode with a simultaneously occurring reduction of ferric iron at the cathode. Both mechanisms are characterized by a negligible thermodynamic threshold.

Their summarized contribution to the overall charge transfer at a defined cell voltage can be determined by linear extrapolation of current values obtained before the onset of the redox-reaction. This procedure is based on the assumption that the electronic contribution is following Ohm's law and is thus linearly correlated to the cell-voltage. The quantified contribution is then subsequently subtracted from the total current i which then yields the "electronic-contribution-corrected" current i_{EC}.

As a third data treatment step, ii-2), the electrolyte's ohmic resistance in the cell (R_{MO}) [Ω] is calculated using the conductivity σ_{MO} [S cm^{-1}] of the electrolyte and the geometrical factor of the cell K following

$$R_{MO} = \frac{K}{\sigma_{MO}} \tag{9}$$

In this study the conductivity is calculated with an empirical model [17] [18] following:

$$ln\sigma_{MO} = \left(19.9 - \frac{47348}{T}\right) \cdot \chi_{Al_2O_3} + \left(9.2 - \frac{14151}{T}\right) \cdot \chi_{MgO} + \left(-0.5 - \frac{7478}{T}\right) \cdot \chi_{SiO_2} + \left(10 - \frac{9140}{T}\right) \cdot \chi_{FeO} \cdot Fe^{2+} + \left(65.4 - \frac{82447}{T}\right) \cdot \chi_{FeO}^2 \cdot Fe^{2+} \cdot Fe^{3+} + \left(-2.6 + \frac{6642}{T}\right) \cdot \chi_{FeO} \cdot Fe^{3+} \tag{10}$$

where χ is the molar fraction of each respective oxide and T the temperature [K]. The obtained values are displayed in Figure 5 for the investigated slags in equilibrium with iron metal. Results obtained with this empirical model are confirmed to a certain extent by independent measurements performed in the base composition without iron [19]. By taking R_{MO} into account, the ohmic drop corrected cell voltage V_{CIR} can be deduced that:

$$\Delta V_{CIR} = \Delta V_E - (i_{EC} R_{MO}). \tag{11}$$

At this point the influence of all parameters of equation (6), except the thermodynamic threshold ΔE_F and the electrode overpotentials, are identified and subtracted from the acquired data. As explained in the introduction, due to the use of the LSA the overpotential of the anode η_A is negligible. ΔV_{CIR} thus displays the response of the cathode overpotential with increasing faradaic current plus the constant contribution of ΔE_F. Identification of the cathode half-reaction will then allow direct quantification the overpotential at the cathode. It has to be noted that by convention the overpotential of the cathode is described in literature by negative values. However, in this study this parameter is derived by measurement of the cell voltage of the entire electrolysis cell. In order to take this into account the overpotential is displayed in this study as absolute values and denoted as $|\Delta V_{CIR}|$.

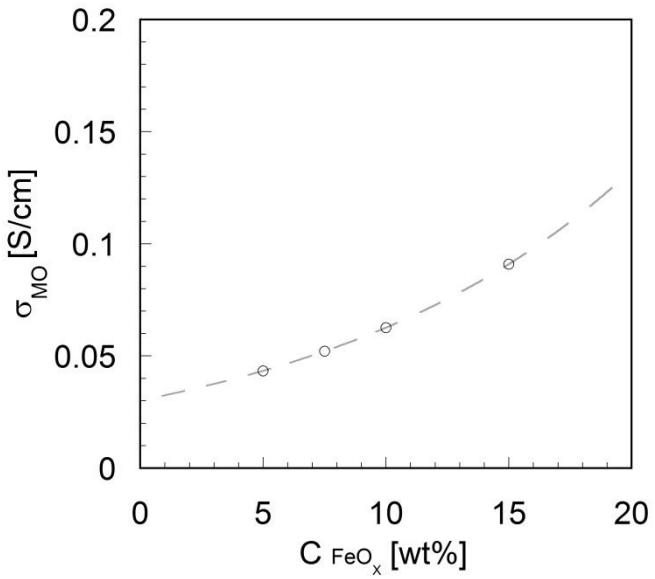

Figure 5: Conductivity of the investigated molten oxides at 1823 K in equilibrium with iron metal calculated following [17] [18] *in dependence of iron oxide concentration; Circles indicate iron concentrations used in this study*

4. Results

Figure 6 shows the untreated current response acquired during the stepped-linear scans. For reasons of reproducibility two experiments were performed for each composition. Differences between the graphs of each composition can be interpreted as slight differences in the positioning of the electrodes. Especially for low iron compositions the difference between the acquired current is marginal. Thus the experiments are considered reproducible. Current linked to the electronic contribution is observed below 0.95 V, it lies between 1 mA and 6 mA with the highest value obtained in Fe#15. In all trials a change in the current slope occurs in the range of 0.95 V to 1.1 V. Thereafter the current shows an exponential trend. A mass transfer limitation, which would be signified by a plateau of the current, is not observed in any of the linear scans. As expected, the current response increases with the cell voltage and the iron concentration.

Measured oxygen level (Figure 7) is characterized by high O_2-levels at the beginning of all the trials. Then a consecutive minimum occurs, with a subsequent rise at high cell voltages. Reactions occurring in the cell cannot be discriminated only by the detection of released oxygen. Indeed, gaseous oxygen can be produced either by a decomposition reaction or an electrochemical reaction at the anode. High O_2 levels at the beginning of the linear scan voltammetry are related to the thermal decomposition of magnetite in the melt [20] [21] via

$$2Fe_3O_4 \leftrightarrows 6FeO + O_2 \qquad (12)$$

In this low cell voltage range, the O_2 flow increases with increasing FeO_x content. The position of the minimum O_2-level depends on the concentration of iron oxides in the melt, which shifts from 1.2 V to higher cell voltages with increasing iron content. For high cell voltage, iron content in the slag has much less influence on the released oxygen level. Rising O_2 values at high cell voltage indicate faradaic charge transfer during oxidation of oxide anion into oxygen gas.

Figure 8 (a) shows the spherical iron deposit produced during the stepped linear scan voltammetry in Fe#10. The transection of the deposit is shown in Figure 8 (b) in a back-scattered electron (BSE) image. The contact with the Pt-10%Rh is seen on the left side of the image, indicated by brighter grey nuances caused by the high content of the two noble elements constituting the wire. The composition of the iron deposit was measured with EDS and is given in Table 2. The high contents of Pt and Rh in the deposit are caused by their diffusion from the cathode wire.

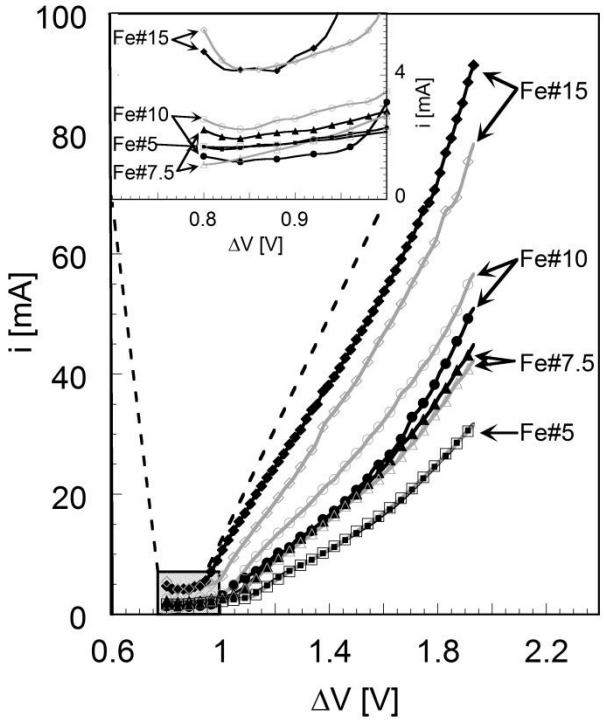

Figure 6: Measured current response during linear scan voltammetry of the electrolytes
Experimental Conditions: 1828 ± 5 K
Potential step: 100 mV – Step duration: 600 s
Ar gas flow: 0.048 STP m^3 h^{-1}

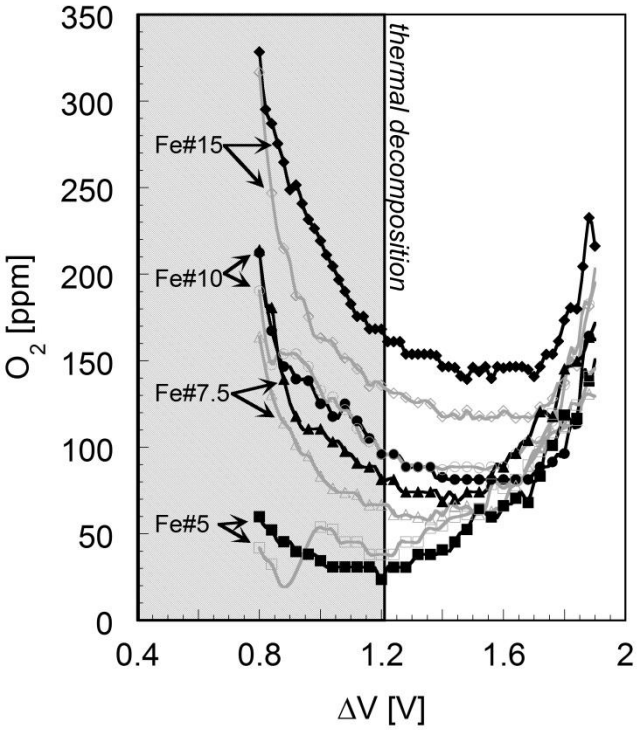

Figure 7: Monitored oxygen response during the conducted experiments
Experimental Conditions: 1828 ± 5 K
Potential step: 100 mV – Step duration: 600 s
Ar gas flow: 0.048 STP m^3 h^{-1}

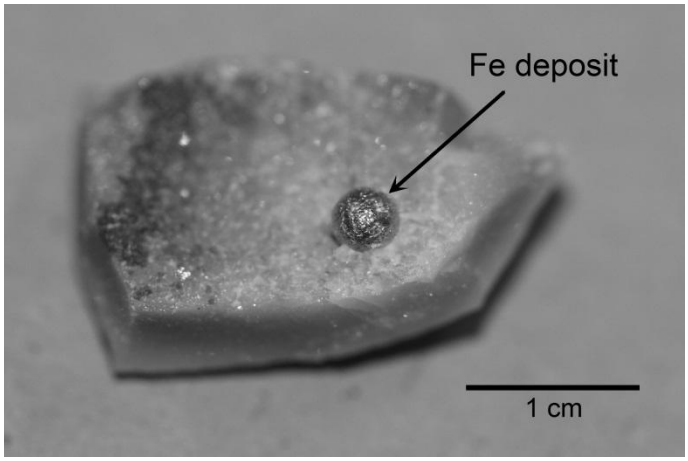

Figure 8 (a): Bottom of the crucible after the linear scan voltammetry with the iron deposit produced in Fe#10

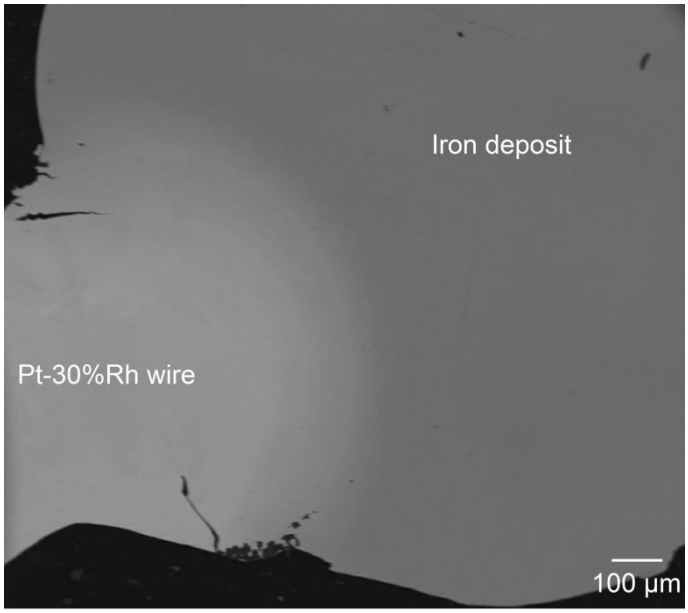

Figure 8 (b): BSE image of the transection of the Fe#10 cathode deposit in contact with the Pt-30%Rh wire
Acceleration voltage: 15 kV

Table 2: EDS analysis of the iron deposit of Fe#10

Element	Average Concentration [wt%]
Fe	66 **±1**
Pt	22 **±2**
Rh	12 **±1**

5. Discussion

5.1. Electronic contribution

As mentioned before, the overall measured current consists of electronic and ionic contributions. This first part of the discussion is aimed to investigate a possible relation between the acquired current signals and the different iron contents in the electrolyte compositions.

The presence of electronic conduction invokes that charges in the molten oxide can be transferred without diffusion of the ions but by electron hopping between stationary ions [22]. The electronic conductivity σ_e of iron bearing glasses is quantitatively described by Mott's equation

$$\sigma_e = \nu_{ph}\left(F^2/RTN_a r\right) exp^{(-2\alpha_{WFD} r)} exp^{(-W/RT)} (\#Fe(III))(1 - \#Fe(III)) \qquad (13)$$

where ν_{ph} is the phonon frequency [s^{-1}]; N_a the Avogadro's number [mol^{-1}]; r the hopping distance [cm]; α_{WFD} the rate of wave function decay [cm^{-1}]; W the activation energy [$J \cdot mol^{-1}$] and *#Fe(III)* the ferric ratio [23] [24].

For the compositions used here, α_{WFD} is unknown, but the difference between the electrolytes can be assumed as negligible since it mainly depends on temperature [24] [25]. Values found in literature are less than 10^{-8} cm^{-1} [23]. The hopping distance (r) can be calculated assuming a homogenous distribution of Fe-ions in the melt following

$$r = N_{Fe}^{(-1/3)} \qquad (14)$$

with N_{Fe} being the number of iron ions per unit volume [25]. Values obtained for the compositions used in this study range from $1.5 \cdot 10^{-7}$ cm in Fe#5 to $9.8 \cdot 10^{-8}$ cm in

Fe#15. Thus the product of α_{WFD} with the hopping distance r in the first exponential term is negligibly low, resulting in a factor of 1, which leads to the assumption of its limited influence on the electronic conduction.

The activation energy "*W*" in unordered systems is governed by the distance between the charge centers, which is equal to the hopping distance (*r*), and is thus varying with the iron concentration. Thus activation energy in molten oxides depends on the iron content [26]. Measurements of this parameter in the investigated composition are not known. Correlation of the electrical activation energy in different compositions with the total iron content suggests that it ranges from 190-200 kJ mol^{-1} [26]. The term $exp^{(-W/RT)}$ thus is expected to vary between $1.9 \cdot 10^{-6}$ and $3.6 \cdot 10^{-6}$. Its variation is non-negligible however it can be directly linked to the total iron content and the ferric ratio in the melt.

According to these considerations on equation (13) the electronic conductivity should then be directly correlated to the ferric ratio (#Fe(III)) and the hopping distance (*r*). Values for the ferric ratio obtained via CEQCSI for the investigated slags are displayed in Table 1. As the ferric ratios are negligibly small in comparison to unity, the second term including the ferric ratio becomes irrelevant to the equation.

Since the geometry of the electrolysis cell is nearly identical between the trials, the only parameter changing from each experiment is the conductivity of the electrolyte. Therefore a possible variation of the total measured current i between the experiments is thus equal to a variation in the electronic conductivity. As shown here the conductivity is only dependent on the total iron concentration which modifies both the ferric ratio and the hopping distance. Thus the measured total current i before the

onset of faradaic charge transfer (potential lower than ~ 1V) is proportional to the ferric ratio and interspatial distance of iron ions *via*

$$i \propto \frac{(\#Fe(III))}{r} \qquad (15)$$

The relationship shows that the electronic conductivity increases with either an increase in the ferric ratio or with a decrease in hopping distance. By plotting the measured total current at an arbitrarily chosen cell voltage below 1 V, here 0.9 V, *vs. #Fe(III)/r* (Figure 9), a linear dependence of eq. (15) is, except for one outlier in Fe#10, confirmed. The error bars depict the standard deviation of the acquired current, which was measured for a period of 10 min in each stepped linear scan voltammetry.

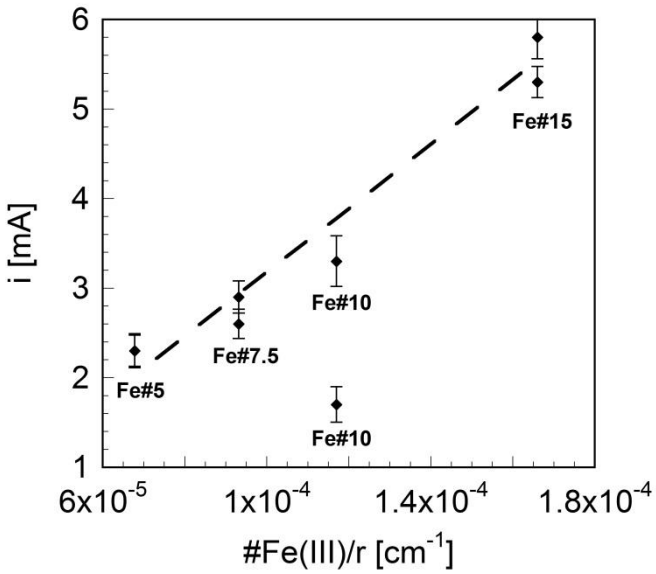

Figure 9: Comparison of the evolution of the conductivity calculated by equation (15) (---) and the currents measured at 0.9 V in the experiments in dependence to the iron oxide concentration (♦). Error bars indicate the standard deviation of the measured currents

5.2. The faradaic current response

The corrected data of the stepped linear scan voltammetry are shown in Figure 10 (a) as absolute values. They take into account the terminal resistance, the ohmic drop

(R_{MO}) and the electronic contribution corrected current (i_{EC}). Only one graph per iron content is shown in order to ease the readability. As mentioned above a diffusional limitation is not detected, yet an even stronger exponential trend is observed compared to the untreated data.

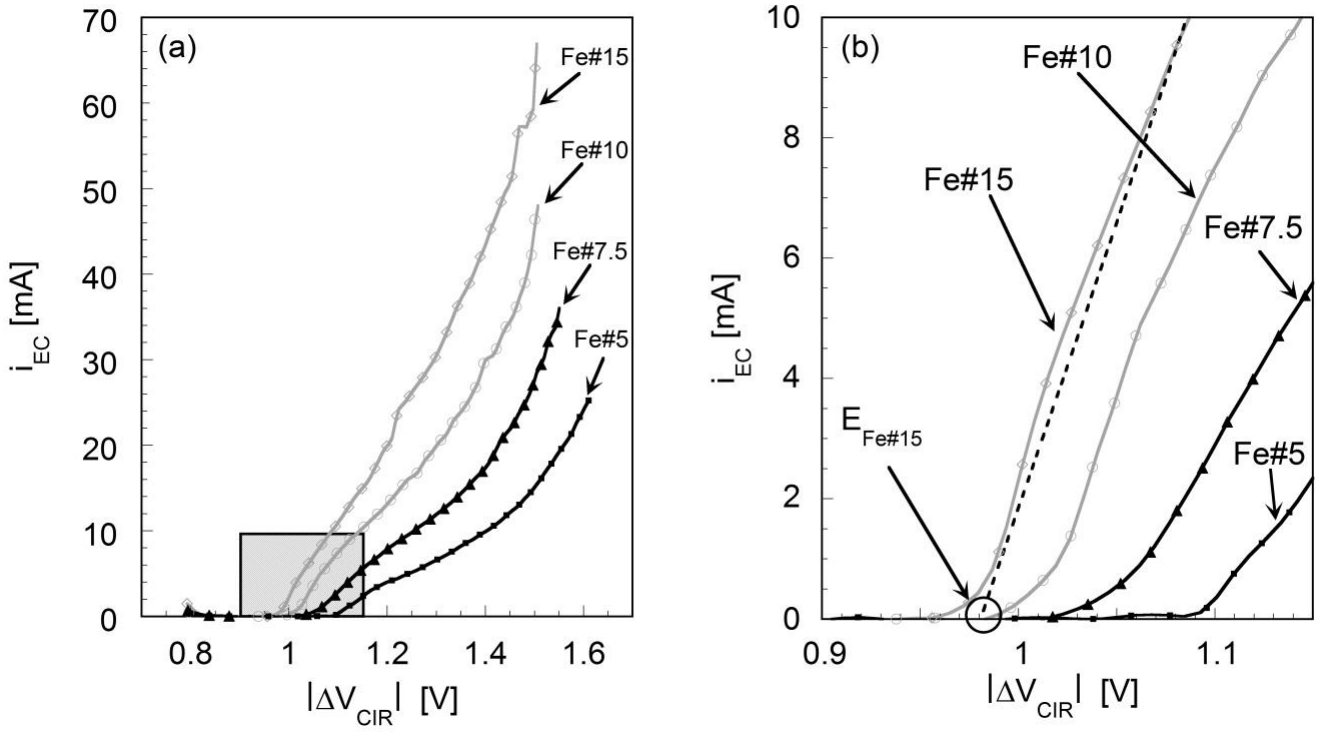

Figure 10: (a) Ohmic drop corrected current response of the corrected cell voltage range $|V_{CIR}|$; the box marks the area of zoom shown in Figure 10 (b)
(b) Magnification on the onset of the potential range of the faradic current onset with illustration of the corresponding reduction potential derivation (b)
Experimental conditions: 1828 ± 5 K; Potential step: 100 mV – Step duration: 600 s;
Ar gas flow: 0.048 STP m^3 h^{-1}

Following the premise to circumvent the use of a reference electrode, the measured current displayed in Figure 10 (a) has been obtained in a two electrode setup with a large surface anode. As described in the introduction this technique allows the determination of the cathode overpotential. Equation (6) is therefore transformed into

$$\eta_C = \Delta V - \Delta E_F - R_T i - R_\Omega i - \eta_A \qquad (16)$$

The thermodynamic threshold ΔE_F is constant and independent of the increasing cell voltage. It is determined by the occurring redox reaction in the cell, which has yet to be identified.

Presuming as described in equation (1) the evolution of O_2 at the anode, possible cathode half-reactions in the investigated potential range are the reduction of ferrous and ferric iron following reaction (2) and (3) at 0.83 V and 0.61 V respectively, as well as the reduction of SiO_2 at 1.51 V following

$$Si(IV) + 4e^- \rightarrow Si \qquad (17)$$

Values for the thermodynamic reduction potentials given here are corresponding to pure compounds, thus with a thermodynamic activity of unity, and are calculated by equation (7) [27]. It can be observed in Figure 10 that in the here performed experiments the potential of 1.51 V is exceeded only at the very end of each stepped linear scan. A significant participation of silica reduction to the total charge transfer can thus be excluded for the interpretation. In addition, Si was not detected in the cathode deposit with the performed EDS analysis, which proves the negligible contribution to the charge transfer of reaction (17). Distinction of the contributions of ferrous and ferric reduction is done by the onset of the faradaic charge transfer which occurs at 1 V. Considering the reduction potential of ferric iron at 0.61 V, still assuming accompanying oxygen production at the anode, the observed onset of current occurs at a too high cell voltage. Thus the reduction of ferric iron is excluded.

As for the anode, two oxidation reactions have to be considered: (i) the formation of $O_{2(g)}$ and (ii) the oxidation of Fe(II) into Fe(III). Although thermodynamically possible, the latter would occur in disagreement with reaction (12) *i.e.* the thermal decomposition of Fe_3O_4. Furthermore the augmentation of O_2 at high cell voltages in

all compositions, as observed in Figure 7, indicates the evolution of O_2-gas due to the anodic half-reaction.

The overall redox-reaction of the cell in the selected conditions is identified as

$$2FeO \rightarrow 2Fe + O_2 \qquad (18)$$

Applying equation (7), taking into account the thermodynamic activities of Fe(II) obtained with the thermochemical software CEQCSI [14], reduction potentials between 0.98 V (Fe#15) and 1.05 V (Fe#5) are calculated. To verify these values it is possible to perform a linear extrapolation of the experimental data just above the current onset (Figure 10b). Linear extrapolation of the slope to a null current provides the thermodynamic potential of the faradaic reaction at the cathode, thus the thermodynamic threshold. Reasoning for this procedure is given by the proximity to the equilibrium potential at vanishingly low currents. Also, any resistance due to the cathodic overpotential is as well vanishingly low due to the low current values. Figure 10 (b) provides a magnified view of the low voltage section. For Fe#15 an example of the procedure described here is given. The dashed line marks the linear extrapolation, the circle envelopes the intersection with the abscissa at which the potential threshold is determined. Via this procedure values of 0.98 V for Fe#15 and 1.08 V for Fe#5 are derived, which correspond well to the potentials calculated beforehand.

All parameters of equations (6) and (16) have now been identified. The graphs in Figure 10 display the current that flows in response to the applied cell voltage solely as a function of the kinetic cathode resistance. The data can then be interpreted following the Tafel interpretation [16]. To do so the results are plotted in logarithmic scale. The result is shown in Figure 11. Subsequent to the onset of the faradaic

charge transfer the measured current increases linearly confirming an interpretation *via* Tafel kinetic. Following this reasoning the overpotential of the cathode η_C is linked to the current by

$$\eta_C = a + b * log(i_{EC}) \quad (19)$$

where $$a = \frac{2.3RT * \log(i_0)}{\alpha F} \quad (20)$$

and $$b = \left|\frac{2.3RT}{-\alpha F}\right| \quad (21)$$

i_0 represents the exchange current [A]. It has to be noted that in general the Tafel approach is validated if linearity for more than one order of magnitude is obtained in logarithmic scale, Figure 11. In the presented data this is not achieved due to the limited scan interval. A deviation from linearity is however not observed which invokes the validity of the Tafel approach and the according interpretation of the results. The absolute values of b are taken as results here are shown as well in absolute values.

By fitting the slope of each composition values of α in the range of 0.54 to 0.66 are obtained. An increase of the iron content leads to a decrease of α. With α = 0.54 the reaction is nearly symmetrical at high concentration. At low concentration the reaction is less symmetric, α = 0.66, and in favor of the electrochemical products. The exchange current i_0 is determined by extrapolating the slope of the linear domain of each composition in Figure 11, to the respective thermodynamic reduction potential of Fe(II) following reaction (18). Values of the derived thermodynamic reduction potentials, transfer coefficients, and the exchange currents are shown in table 3 for the different electrolyte compositions.

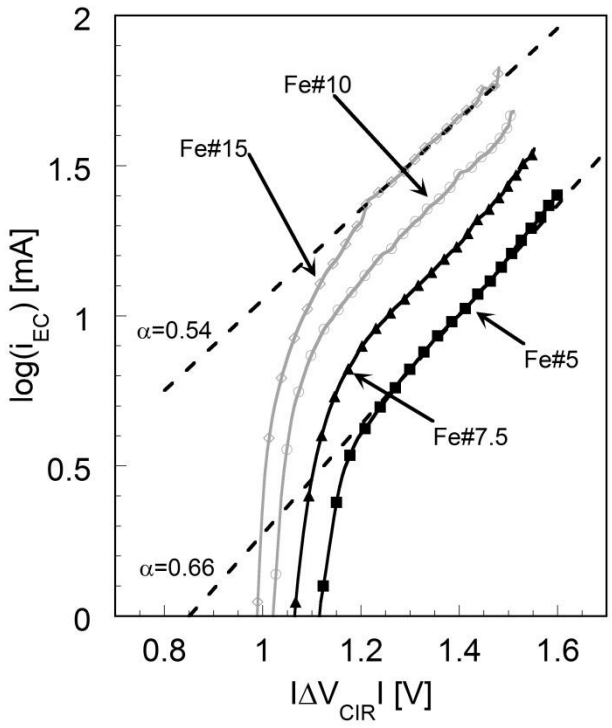

Figure 11: Tafel interpretation of the treated measurements
Experimental conditions: 1828 ± 5 K
Potential step: 100 mV – Step duration: 600 s
Ar gas flow: 0.048 STP $m^3 \cdot h^{-1}$

Table 3: Values of the experimentally derived thermodynamic reduction potential, the reaction transfer coefficients and the exchange currents

	Thermodynamic reduction potential **[V]**	Transfer coefficient	Exchange current **[mA]**
Fe#5	1.08	0.66	3.1
Fe#7.5	1.03	0.65	4.5
Fe#10	0.99	0.61	6.8
Fe#15	0.98	0.54	11.1

In order to calculate the current density j_0 from the exchange current i_0, it is assumed that the surface of the cathode does not significantly change during the duration of

the experiment (560 min). Results are plotted in Figure 12 as a function of the iron oxide content. The order of reaction is then determined by the degree of the power law and is obtained by fitting a log-log plot. For the results presented in this study the order of reaction is determined as 1.1. Taking into account possible deviations in the cell geometry between each experiment and operating conditions it is probable that the order of reaction is close to unity and thus solely depending on the Fe(II) concentration.

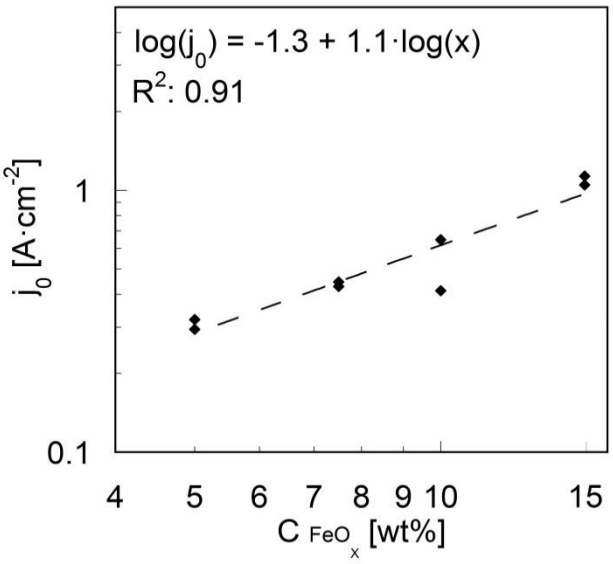

Figure 12: Exchange current density in dependence of the iron concentration
Experimental Conditions: 1823 ± 5 K
Potential step: 100 mV – Step duration: 600 s
Ar gas flow: 0.048 STP $m^3 \cdot h^{-1}$

6. Conclusion

Results presented in this work demonstrate that metal deposition at very high temperature by electrochemistry can be achieved and studied quantitatively. A dedicated device was designed to carry out iron metal production under controlled conditions of potential which is the driving force of the process. Control of the electrochemical potential in the experimental device was achieved by means of a large surface electrode. Performing an ohmic drop correction of the herewith acquired electrochemical signal allowed then the quantification of the kinetics of the cathode half-reaction.

The produced iron deposit at the cathode shows a high purity. In the investigated range of iron concentrations a diffusional rate limitation is not observed. The limiting step of the cathode half-reaction is therefore the reaction kinetics of the reduction process at the cathode. Interpretation of the results using Tafel yields transfer coefficients of 0.54 to 0.66 with an order of reaction close to unity.

7. Acknowledgement

The authors wish to acknowledge the French Agency for the Environment and Energy Management (ADEME) for the financial support. We are grateful to Mr. Jean Lehmann for the numerous discussions and the valuable suggestions during the preparation of this study. Also the authors wish to thank Ms. Perrine Tanguy for her skillful analysis of the samples at the electron microscope.

8. References

[1] A. Allanore, "Features and challenges of molten oxide electrolytes for metal extraction," *Journal of Electrochemical Society,* vol. 162, pp. E13-E22, 2015.

[2] U. B. Pal, "A lower carbon footprint process for production of metals from their oxide sources," *Journal of Metals,* vol. 2, pp. 43-47, 2008.

[3] L. Hashkin, R. Colson , D. Lindstrom, R. Lewis and K. Semkov, "Electrolytic smelting of lunar rock for oxygen, iron and silicon," *Proceedings of the 2nd conference on lunar bases and space acivities,* pp. 411-422, 1992.

[4] A. Allanore, L. Yin and D. R. Sadoway, "A new anode material for oxygen evolution in molten oxide electrolysis," *Nature,* vol. 497, pp. 353-357, 2013.

[5] D. Wang, A. Gmitter and D. R. Sadoway, "Production of oxyen gas and liquid metal by electrochemical decomposition of molten iron oxide," *Journal of Electrochemical Society,* vol. 158, pp. E51-E54, 2011.

[6] H. Kim, J. Paramore, A. Allanore and D. R. Sadoway, "Electrolysis of molten iron oxide with an iridium anode: the electrolyte basicity," *Journal of Electrochemical Society,* vol. 158, pp. E101-E105, 2011.

[7] A. Sirk, D.R. Sadoway and L. Sibille, "Direct electrolysis of molten lunar regolith for the production of oxygen and metals on the moon," *ECS Transactions,* vol. 28, no. 6, pp. 367-273, 2010.

[8] D. Wang, A. Gmitter and D.R. Sadoway, "Production of oxygen gas and liquid metal by electrochemical decomposition of molten iron oxide," *Journal of the Electrochemical Society,* vol. 158, no. 6, pp. E51-E54, 2011.

[9] E. T. Turkdogan, "The physicochemical properties of molten slags and glasses," *The Metals Society,* 1983.

[10] W. E. Haupin, "Principles of aluminum electrolysis," *Light Metals 1995,* pp. 195-203, 1995.

[11] R. Moretti and G. Ottonello, "Polymerization and disproportionation of iron and sulfur in silcate melts: insights from an optical basicity-based approach," *Journal of Non-Crystalline Solids,* vol. 323, pp. 111-119, 2003.

[12] B. O. Mysen, D. Virgo and F. Seifert, "Redox equilibria of iron in alkaline earth silicates: relationships between melt structure, oxygen fugacity, temperature and properties of iron-bearing silicate liquids," *American Mineralogist,* vol. 69, pp. 834-847, 1984.

[13] G. Ottonello, R. Moretti, L. Marini and M. Vetuschi Zuccolini, "Oxidation state of iron in silicate glasses and melts: a thermochemical model," *Chemical Geology,* vol. 174, pp. 157-159, 2001.

[14] C. Gatellier, H. Gaye, J. Lehmann and Y. Zbaczyniak, "Des outils thermodynamiques pour la maîtrise des réactions métal-laitier et le controlôle inclusionnaire des aciers," *Revue de Metallurgie,* pp. 887-888, 1992.

[15] F. Stouvenot et H. Gaye, «Masse volumique. viscosité. tension superficielle et interfaciale des métaux. alliages et oxydes liquides.,» *Internal Report* ArcelorMittal, Maizières-lès-Metz, 1995.

[16] A. Bard, L. Faulkner, J. Leddy and C. Zoski, "Electrochemical methods: fundamentals and applications," vol. 2, 1980.

[17] R. Hundermark, "The electrical conductivity of melter type slags," *Master's thesis,* 2003.

[18] G. Georgalli, J. Eksteen, R. Bezuidenhout, B. Van Beek and T. Goff, "Towards electrode immersion control on Lonmin's No.1 circular furnace," *Proceedings: Third International Platinum Conference, Platinum in Transformation, The Southern African Instiute of Mining and Metallurgy,* pp. 219-230, 2008.

[19] J. H. Downing and L. Urban, "Electrical conduction in submerged arc-furnaces," *Journal of Metals,* pp. 337-344, 1966.

[20] L. S. Darken and R. W. Gurry, "The system iron-oxygen. Equilibrium and thermodynamics of liquid oxide and other phases," *Journal of American Chemical Society,* vol. 68, pp. 798-816, 1946.

[21] A. G. Crouch, K. A. Hay and R. T. Pascoe, "Magnetite-Haematite-liquid equilibrium conditions at oxygen pressures up to 54 bar," *Nature Physical Science,* vol. 234, pp. 132-133, 1971.

[22] H. Inouye, J. W. Tomlinson and J. Chipman, "The electrical conductivity of wüstite melts," *Transactions of the Faraday Society,* vol. 49, pp. 796-801, 1953.

[23] N. Mott, "Electrons in disordered structures," *Advances in Physics,* vol. 50, no. 7, pp. 865-945, 2001.

[24] L. Murawski, C. H. Chung and J. D. Mac Kenzie, "Electrical properties of semiconducting oxide glasses," *Journal of Non-Crystalline Solids,* vol. 32, pp. 91-104, 1979.

[25] M. Barati and K. S. Coley, "Electrical and electronic conductivity of $CaO-SiO_2-FeO_x$ slags at various oxygen potentials. Part II: Mechanism and a model of electronic conduction," *Metallurgical and Materials Transactions B,* vol. 37B, pp. 51-60, 2006.

[26] M. Barati et K.S. Coley, «Electrical and electronic conductivity of $CaO-SiO_2-FeO_x$ slags at various oxygen potentials: Part 1. Experimetal results,» *Metallurgical and Materials Transactions B,* vol. 37B, pp. 41-49, 2006.

[27] I. Barin, "Thermochemical data of pure substances," *Wiley-VCH,* 2004.